

A HODGKIN–HUXLEY MODEL EXHIBITING
BURSTING OSCILLATIONS

Paul R. Shorten and David J.N. Wall

*Biomathematics Research Centre,
Department of Mathematics & Statistics,
University of Canterbury,
Private Bag 4800, Christchurch, New Zealand.*

Report Number: 187

December 1999

Keywords: Bifurcations, Calcium, Corticotrophs, Endoplasmic reticulum

A Hodgkin–Huxley model exhibiting bursting oscillations

Paul R. Shorten * David J.N. Wall *

December 1999

Abstract

We investigate bursting behaviour generated in an electrophysiological model of pituitary corticotrophs. The active and silent phases of this mode of bursting are generated by moving between two stable oscillatory solutions. The bursting is indirectly driven by slow modulation of the endoplasmic reticulum Ca^{2+} concentration. The model exhibits different modes of bursting, and we investigate mode transitions and similar modes of bursting in other Hodgkin–Huxley models. Bifurcation analysis and the use of null-surfaces facilitate a geometric interpretation of the model bursting modes and action potential generation respectively.

1 Introduction

A Hodgkin–Huxley type mathematical model has been constructed which includes the major plasma membrane ionic currents identified in pituitary corticotrophs and the associated intracellular Ca^{2+} dynamics [LeBeau et al., 1997, Shorten et al., 1999a]. In certain parameter regimes the model exhibits a novel form of bursting behaviour. This bursting is due to the existence of a fast time scale associated with the membrane action potentials and a slow time scale associated with the slow modulation of the endoplasmic reticulum (ER) Ca^{2+} concentration. In this paper we investigate this bursting where the quiescent state is a small amplitude (“subthreshold”) limit cycle attractor and the spiking state is a limit cycle attractor. In order to perform a mathematical analysis of this bursting behaviour we study a reduced version of this model which also exhibits topologically similar types of bursting behaviour in certain parameter regimes.

Although pituitary corticotrophs do not seem to exhibit these modes of bursting this interesting type of bursting hasn’t been observed in Hodgkin–Huxley type models and warrants further study. Some corticotrophs exhibit other modes of bursting where the depolarization spike is followed by small oscillations in the membrane potential [Kuryshv et al., 1996,

*Biomathematics Research Centre, Department of Mathematics & Statistics, University of Canterbury, Private Bag 4800, Christchurch 1, New Zealand.

Kuryshv et al., 1997, Adler et al., 1983]. These modes of bursting are exhibited in our model and the behaviour and underlying mechanisms have previously been investigated [LeBeau et al., 1998, Shorten et al., 1999b].

The bursting process is driven by the slow modulation of the endoplasmic reticulum Ca^{2+} concentration ($[\text{Ca}^{2+}]_{\text{er}}$), giving rise to a slow component in $[\text{Ca}^{2+}]_i$. This slow component in $[\text{Ca}^{2+}]_i$ gives rise to the electrical bursting via a Ca^{2+} -activated K^+ current. This store operated burst modulation mechanism has also been observed in other Hodgkin–Huxley type models [Chay, 1997, Gall and Susa, 1999], and we analyse this mechanism from a bifurcation perspective.

There has been much interest in bursting oscillations in electrophysiological systems based on slowly varying dynamical systems [Rinzel, 1987, Bertram et al., 1995, de Vries, 1998]. There are two time scales identified in our model; a fast time scale associated with membrane action potentials, and a slow time scale associated with the gradual increase in $[\text{Ca}^{2+}]_{\text{er}}$. This slow time scale allows us to interpret the model as a fast system evolving through a slow subsystem. Thus by treating the slow variable as a fixed parameter the system can be regarded as a family of vector fields. This allows the use of tools from bifurcation theory to investigate the modes of bursting in the model.

The first formal classification of bursting is due to Rinzel (1987) who classified the “parabolic”, “elliptic”, and “square-wave” modes of bursting. Bertram et al. (1995) suggested using Roman numerals to identify the different modes, and they introduced the Type IV burster. Further classification was also carried out by Rush and Rinzel (1994) and de Vries (1998) who suggested the addition of the “triangular” and Type V burster respectively. However the current naming scheme is misleading and is becoming unmanageable as the number of classified modes increases. A more self-explanatory comprehensive naming scheme suggested by Izhikevich (2000) is to name the bursting mode after the two bifurcations involved. Thus for example the well known “elliptic” (Type III) burster is a “subHopf/fold cycle” burster because the rest state disappears in a subcritical Hopf bifurcation and the limit cycle attractor disappears in a fold limit cycle bifurcation. All of the aforementioned bursters are termed point–cycle bursters due to the fact that the quiescent state is a stable equilibrium and the spiking state is a limit cycle attractor. In this paper we investigate a novel form of bursting due to bistability between two periodic solutions. This is termed a cycle–cycle burster. Due to the bifurcations involved, this topological type of bursting is named “fold cycle/fold cycle” bursting [Izhikevich, 2000]. Because the fast spiking subsystem is two-dimensional the burster is termed planar by Izhikevich (2000).

The model bursting is similar to a mode of cycle–cycle bursting exhibited in the neuron model of Wang (1993). However in that model the bursting is modulated by the slow inactivation kinetics of a K^+ current. We show here a bifurcation analysis with respect to this inactivation variable which reveals the model bistability. This shows the subthreshold limit cycle disappears in a fold cycle bifurcation and the spiking limit cycle attractor disappears in a subcritical flip (period doubling) bifurcation. This mode is termed a “fold cycle/flip” burster [Izhikevich, 2000].

The broad classification scheme of Izhikevich (2000) is theoretical in the sense that many of the 120 bursting modes have yet to be observed in conductance based models.

The “fold cycle/fold cycle” and “fold cycle/flip” bursters identified in our paper have not previously been observed in Hodgkin–Huxley type models. An interesting open problem is whether conductance based models of the Hodgkin–Huxley type impose restrictions on the possible bifurcations and hence the type of bursters [Izhikevich, 2000].

2 The model

The model is of Hodgkin–Huxley form [Hodgkin and Huxley, 1952], and consists of seven coupled ordinary differential equations. Four ionic currents are included in the model: 1) a high-voltage threshold dihydropyridine-sensitive L-type Ca^{2+} current ($I_{\text{Ca-L}}$), responsible for most of the inward Ca^{2+} current during an action potential; 2) a low-voltage threshold rapidly inactivating T-type voltage-sensitive Ca^{2+} current ($I_{\text{Ca-T}}$); 3) a voltage-sensitive K^+ current ($I_{\text{K-DR}}$), predominantly responsible for the action potential repolarization; and 4) a Ca^{2+} -activated K^+ current ($I_{\text{K-Ca}}$), essential in the bursting behaviour. The remaining leak current (I_{Leak}) represents all other ionic current contributions not specifically described. The construction of these ionic currents from electrophysiological measurements in corticotrophs has previously been described in LeBeau et. al., (1997). The resulting equations and parameters are shown in the Appendix.

Ca^{2+} transport is crucial for action potential generation in corticotrophs, and the model includes equations for the intracellular Ca^{2+} concentration ($[\text{Ca}^{2+}]_i$) and the ER Ca^{2+} concentration. The ER performs a number of important cellular functions, including cellular Ca^{2+} homeostasis and protein synthesis [Alberts et al., 1983, p335]. A schematic diagram of the ionic transport processes is shown in Fig. 1.

The bursting type behaviour we discuss and analyse is exhibited in the full seven variable model and simpler models containing a smaller number of variables, albeit with slightly different parameter values. The reduction in the number of model variables utilises the fact that the channel gating variables m_L , h_T and m_T present in the $I_{\text{Ca-L}}$ and $I_{\text{Ca-T}}$ channel currents (see the Appendix) remain very close to their steady state values during an action potential, that is they are fast variables and can be removed and set to their steady state values. This produces a four variable model, which has been previously discussed in the context of action potential generation and excitability [LeBeau et al., 1998]. However for ease of explanation we eliminate another variable from the model. The fourth gating variable n , present in the $I_{\text{K-DR}}$ channel current (see the Appendix), is not as fast as the membrane potential difference (V). However to aid in the visualisation of the model we set n to its steady state value to obtain the three variable model governed by the equations in Table 1. This change does not significantly change the model dynamics. This model system was solved using a stiff system solver in the numerical package XPPAUT(3.0)¹. Bifurcation diagrams were computed using AUTO [Doedel, 1981], as incorporated in XPPAUT.

¹Written by Bard Ermentrout, and available at <ftp.math.pitt.edu/pub/bardware>

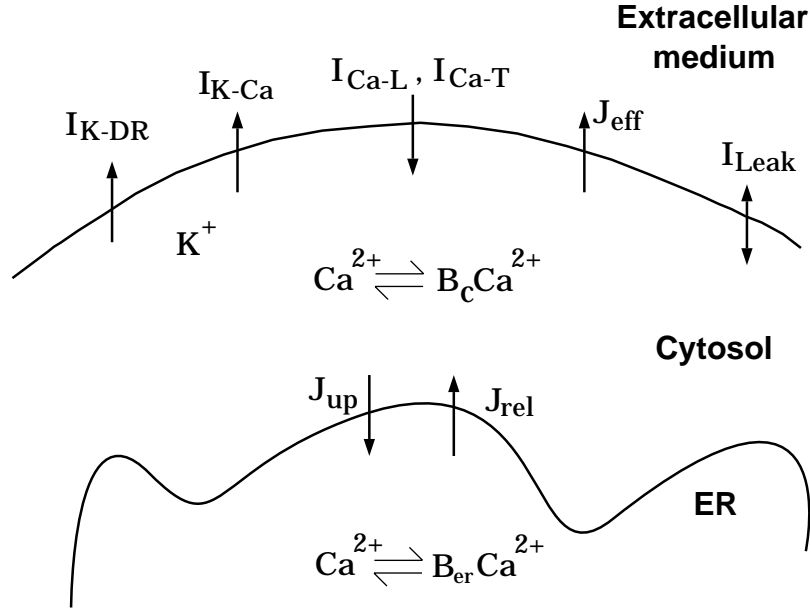


Figure 1: Schematic diagram of the ionic pathways included in the model. Three compartments are distinguished, the cytosol, the ER, and the extracellular medium. Arrows indicate ionic channels and pumps. Within the ER and cytosolic compartments, significant portions of Ca^{2+} are bound to buffers, denoted by B_{er} and B_{c} respectively. Four ionic currents are included in the model: an L-type voltage-sensitive Ca^{2+} current $I_{\text{Ca-L}}$, a fast inactivating T-type voltage-sensitive Ca^{2+} current $I_{\text{Ca-T}}$, a voltage-sensitive K^+ current $I_{\text{K-DR}}$, and a non-voltage sensitive Ca^{2+} -activated K^+ current $I_{\text{K-Ca}}$. The remaining leak current I_{Leak} represents all other ionic current contributions. Also indicated are the ER and plasma membrane Ca^{2+} -ATPase pumps, J_{eff} and J_{up} respectively, along with an ER Ca^{2+} leakage term J_{rel} .

$$\begin{aligned}
 c_m \frac{dV}{dt} &= -(I_{\text{Ca-L}} + I_{\text{Ca-T}} + I_{\text{K-DR}} + I_{\text{K-Ca}} + I_{\text{Leak}}), \\
 \frac{d[\text{Ca}^{2+}]_i}{dt} &= \frac{f_{\text{cyt}}}{V_{\text{c}}} (J_{\text{rel}} - J_{\text{up}}) + f_{\text{cyt}} \beta (J_{\text{in}} - J_{\text{eff}}), \\
 \frac{d[\text{Ca}^{2+}]_{\text{er}}}{dt} &= -\frac{f_{\text{er}}}{V_{\text{er}}} (J_{\text{rel}} - J_{\text{up}}), \\
 x &= x_{\infty}(V), \quad x \in \{m_{\text{L}}, m_{\text{T}}, h_{\text{T}}, n\},
 \end{aligned}$$

Table 1: Reduced three-variable model equations.

3 The model bursting

The bursting behaviour in the three variable model is shown in Fig. 2 A. The quiescent state is a small amplitude (“subthreshold”) limit cycle attractor and the spiking state is a limit cycle attractor. Due to the bistability between two periodic solutions this is termed a cycle-cycle burster [Izhikevich, 2000]. The silent and active phases of the bursts are associated with increasing and decreasing $[\text{Ca}^{2+}]_{\text{er}}$ respectively (Fig. 2 C).

During the spiking train of action potentials $[\text{Ca}^{2+}]_{\text{er}}$ slowly increases as the ER sequesters Ca^{2+} and therefore acts to buffer the $[\text{Ca}^{2+}]_{\text{i}}$ (Fig. 2 C). If only a single $[\text{Ca}^{2+}]_{\text{i}}$ transient was generated, the additional ER Ca^{2+} would be returned to the cytosol, and eventually removed from the cell altogether to recover cellular $[\text{Ca}^{2+}]$ homeostasis. However, Fig. 2 C shows that with each successive action potential, $[\text{Ca}^{2+}]_{\text{er}}$ builds up as each transient contributes additional Ca^{2+} to the cytosol via the L-type Ca^{2+} current. $[\text{Ca}^{2+}]_{\text{er}}$ increases until $[\text{Ca}^{2+}]_{\text{er}} = 17.8 \mu\text{M}$, where the limit cycle disappears and $[\text{Ca}^{2+}]_{\text{er}}$ begins to decrease. The trajectory is then attracted towards the smaller stable subthreshold quiescent state. $[\text{Ca}^{2+}]_{\text{er}}$ decreases until $[\text{Ca}^{2+}]_{\text{er}} = 17.3 \mu\text{M}$, where the small periodic orbit disappears, and the trajectory is attracted back towards the spiking state. The process of moving between the two stable periodic solutions then repeats, and we obtain “fold cycle/fold cycle” bursting behaviour. The “fold cycle/fold cycle” bursting can be visualised as a flow on a two-dimensional invariant torus in V - $[\text{Ca}^{2+}]_{\text{i}}$ - $[\text{Ca}^{2+}]_{\text{er}}$ phase space [Hale and Kocak, 1991], with the silent and active phases of the bursts associated with flow on the inner and outer surfaces of the torus, respectively.

The $[\text{Ca}^{2+}]_{\text{i}}$ transients mimic the voltage bursting response (Fig. 2 B). Coupled to the increase in $[\text{Ca}^{2+}]_{\text{er}}$ during the spiking phase is a slight rise in the average $[\text{Ca}^{2+}]_{\text{i}}$ (i.e., averaged over the course of a transient) The small rise in $[\text{Ca}^{2+}]_{\text{i}}$ results from an enhanced Ca^{2+} leak current from the ER and leads to a gradual increase in the average activation of $I_{\text{K-Ca}}$. This in turn has a subtle inhibitory effect on the regeneration of action potentials. During the spiking phase the action potential peaks slightly decrease until enough feedback is present to significantly reduce the action potentials, resulting in small amplitude oscillations. To allow the individual action potentials to be resolvable on the scale illustrated, the ER Ca^{2+} buffering factor is increased from $f_{\text{er}} = 0.0025$ to $f_{\text{er}} = 0.01$. This reduction in the ER Ca^{2+} buffering allows $[\text{Ca}^{2+}]_{\text{er}}$ to change more rapidly and has little effect on the dynamics under consideration.

The bursting is modulated by a very minor increase in $[\text{Ca}^{2+}]_{\text{i}}$, demonstrating the delicate interplay between the ER filling state and the plasma membrane electrical activity. This store operated burst modulation mechanism has also been observed in other Hodgkin–Huxley type models [Chay, 1997, Gall and Susa, 1999]. Further, this effect shows that the ER could potentially play an important signaling role despite an initial appearance that it plays only a passive, buffering function during CRH-induced activity.

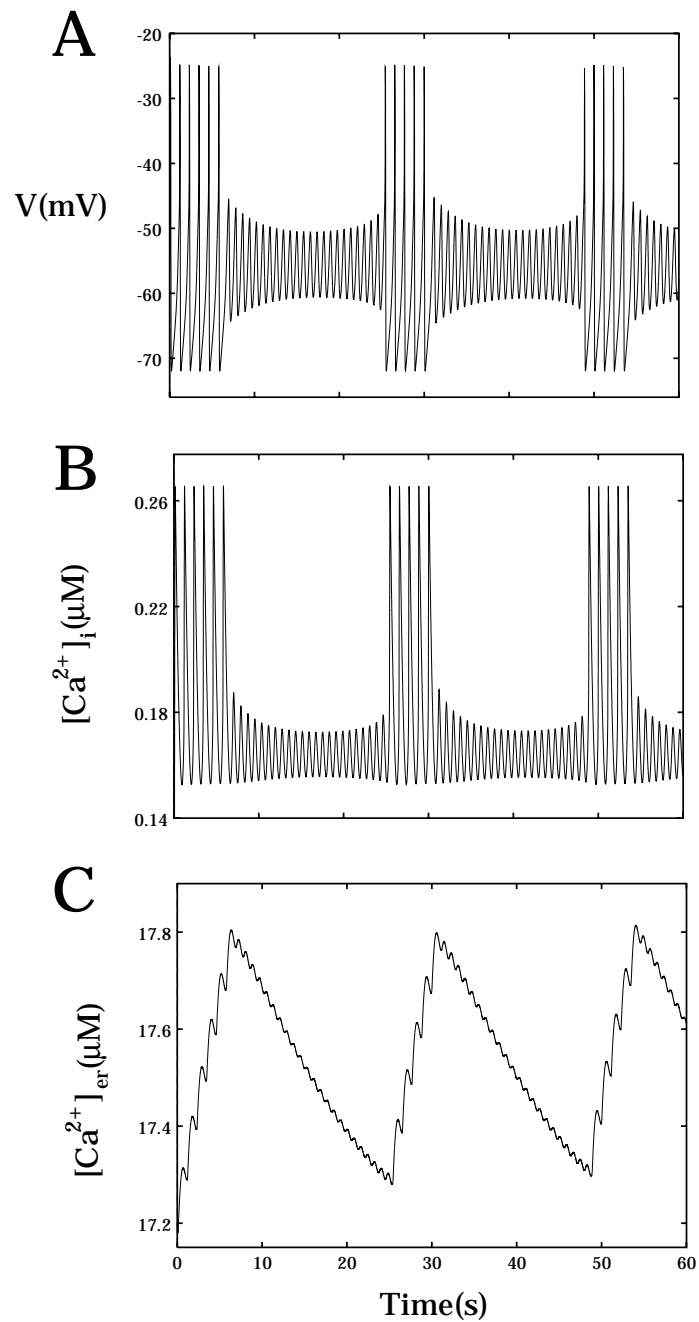


Figure 2: (A) Model “Fold cycle/fold cycle” bursting due to bistability between the two stable periodic solutions. To allow the individual action potentials to be resolvable on the scale illustrated, the ER Ca^{2+} buffering factor is increased from $f_{\text{er}} = 0.0025$ to $f_{\text{er}} = 0.01$. (B) Coupled to the voltage bursting response are $[\text{Ca}^{2+}]_i$ transients. (C) During the active and silent phases of the bursts $[\text{Ca}^{2+}]_{\text{er}}$ increases and decreases respectively.

4 One parameter bifurcation analysis

Now we consider a fast-slow decomposition of the system of equations based on the pioneering work of Rinzel (1985, 1986, 1987). This decomposition is justifiable since the spiking time scale is significantly smaller than the time scale of modulation. As illustrated in Fig. 2, it is evident that V and $[Ca^{2+}]_i$ are the fast variables, and $[Ca^{2+}]_{er}$ is the slow variable. By treating the slow variable $[Ca^{2+}]_{er}$ as a fixed parameter we can interpret the model as a family of vector fields, with the slow variable dynamics allowing the fast system to evolve through this family.

We illustrate the sequence of model behaviour by showing trajectories in $[Ca^{2+}]_i$ - V phase space instead of temporal plots. If the slow variable $[Ca^{2+}]_{er}$ is fixed at $17 \mu\text{M}$ then the model exhibits stable action potentials as shown by the stable periodic orbit (—) in Fig. 3 A. Increasing $[Ca^{2+}]_{er}$ to $17.6 \mu\text{M}$ changes the model behaviour. In addition to the large stable periodic orbit a smaller stable oscillation has emerged as shown in Fig. 3 B. In between these two stable periodic solutions lies an unstable periodic orbit (---). This unstable periodic orbit specifies the regions of attraction of the two periodic solutions. If $[Ca^{2+}]_{er}$ is further increased the model behaviour changes again. Fig. 3 C indicates the model behaviour when $[Ca^{2+}]_{er} = 18 \mu\text{M}$. The large periodic orbit has coalesced with the unstable periodic orbit and disappeared. All trajectories are now attracted onto the smaller stable periodic orbit. If $[Ca^{2+}]_{er}$ is further increased to $[Ca^{2+}]_{er} = 19 \mu\text{M}$, then the small stable periodic solution has disappeared, and all trajectories are attracted onto a stable steady state solution (Fig. 3 D). The sequence of $[Ca^{2+}]_{er}$ values chosen above are not values for which bifurcations occur.

The visualisation of the vector field is useful in understanding the model behaviour. This is the reason we make the reduction to the three variable model. The nullclines are helpful in understanding action potential generation, and are shown with $[Ca^{2+}]_{er}$ fixed at $17 \mu\text{M}$ in Fig. 3 A. The S-shaped V nullcline (\cdots) is not a function of $[Ca^{2+}]_{er}$, and hence is simple to visualise. However the $[Ca^{2+}]_i$ nullcline (---) is a function of $[Ca^{2+}]_{er}$, and moves gradually up and to the left with increasing $[Ca^{2+}]_{er}$ (see Fig. 3 D). Superimposed in Fig. 3 A is the orbit of a typical action potential (—) in the V - $[Ca^{2+}]_i$ phase plane. Notice that the orbit is heavily attracted onto the S-shaped V nullcline, indicating that V is a faster variable than $[Ca^{2+}]_i$.

To summarise the sequence of phase portraits shown in Fig. 3 a bifurcation analysis of the model with respect to the slow variable $[Ca^{2+}]_{er}$ is shown in Fig. 4 A. This bifurcation structure is called the slow manifold. For $[Ca^{2+}]_{er} < 17.46 \mu\text{M}$ the model only exhibits stable action potentials (—), with an amplitude of about 50 mV. However for $17.46 \leq [Ca^{2+}]_{er} < 17.76 \mu\text{M}$ the model exhibits bistability due to the emergence of a small stable solution from a saddle node of periodics bifurcation (SNP). A SNP bifurcation is also called a fold bifurcation of limit cycles or a fold cycle, the term we use in our classification of bursting. The unstable periodic orbit (---) denotes the regions of attraction of the two periodic orbits. For $17.76 \leq [Ca^{2+}]_{er} < 18.29 \mu\text{M}$ only small oscillations are exhibited due to the disappearance of the action potentials through another SNP bifurcation. For $[Ca^{2+}]_{er} \geq 18.29 \mu\text{M}$ the small oscillations disappear in a supercritical Hopf bifurcation

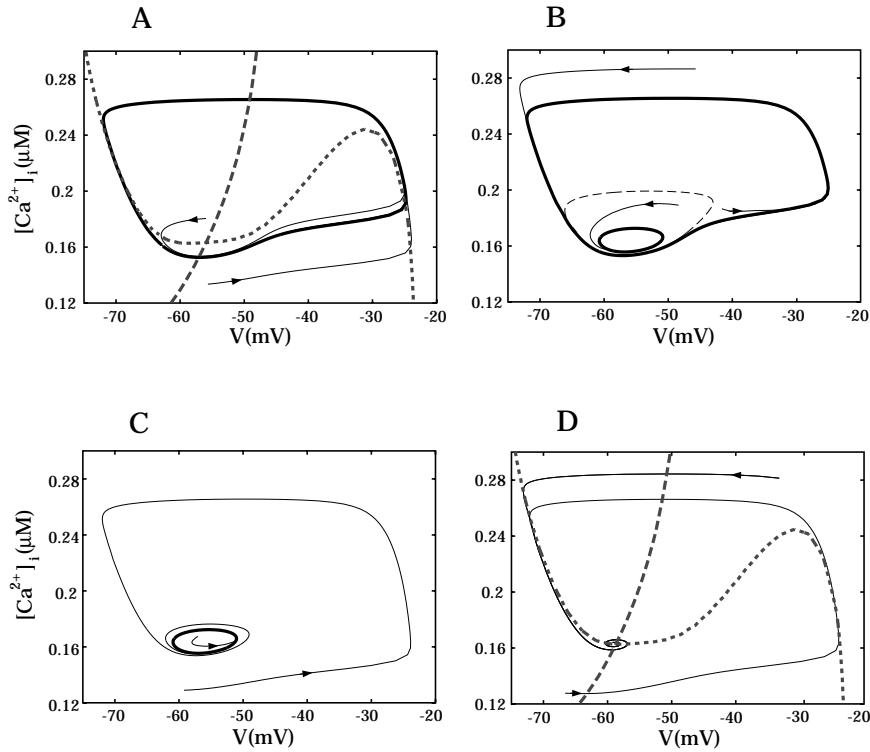


Figure 3: Sequence of model situations as $[\text{Ca}^{2+}]_{\text{er}}$ increases. (A) For $[\text{Ca}^{2+}]_{\text{er}} = 17 \mu\text{M}$ the model exhibits stable action potentials (—). The S-shaped V nullcline ($\cdot\cdot\cdot$) and the $[\text{Ca}^{2+}]_{\text{i}}$ nullcline (---) indicate that V is a faster variable than $[\text{Ca}^{2+}]_{\text{i}}$. Directed arrows represent trajectories. (B) For $[\text{Ca}^{2+}]_{\text{er}} = 17.6 \mu\text{M}$ a small stable oscillation has emerged that is surrounded by an unstable periodic orbit (---). (C) The larger periodic orbit has coalesced with the unstable periodic orbit and disappeared when $[\text{Ca}^{2+}]_{\text{er}} = 18 \mu\text{M}$. (D) When $[\text{Ca}^{2+}]_{\text{er}} = 19 \mu\text{M}$ the small stable periodic solution has disappeared and is replaced by a single stable steady state.

(HB) and the previous unstable steady state (---) becomes stable (—). The interesting feature of Fig. 4 A is the bistability between two stable periodic solutions for $[\text{Ca}^{2+}]_{\text{er}}$ between the two SNP bifurcations. It is this bistability that is critical for the bursting type behaviour in the model.

The $[\text{Ca}^{2+}]_{\text{er}}$ null-surface is independent of V , and is relatively linear for $[\text{Ca}^{2+}]_{\text{er}} < 20 \mu\text{M}$. This null-surface is easily visualised and seems simple, but the way it interacts with the other two null-surfaces leads to interesting behaviour. This interaction is shown in Fig. 4 A, where the $[\text{Ca}^{2+}]_{\text{er}}$ nullcline ($\cdot\cdot\cdot$) is superimposed onto the slow manifold. This diagram is useful in understanding of the bursting behaviour previously shown in Fig. 2 A.

The bursting oscillations result from bistability between two stable periodic solutions, with the silent and active phases of the bursts associated with increasing and decreasing $[\text{Ca}^{2+}]_{\text{er}}$ respectively (see Fig. 2). During the spiking train of action potentials $[\text{Ca}^{2+}]_{\text{er}}$ increases until $[\text{Ca}^{2+}]_{\text{er}} = 17.76 \mu\text{M}$, the upper SNP bifurcation in Fig. 4 A. The trajectory is

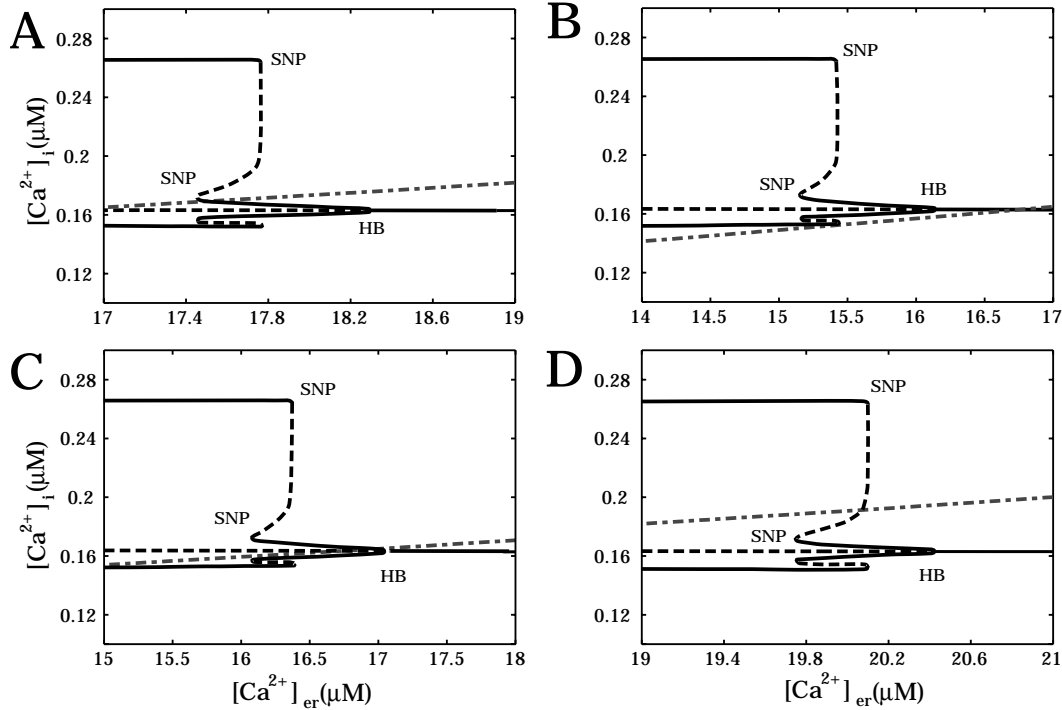


Figure 4: Model $[\text{Ca}^{2+}]_{\text{er}}$ nullcline ($\cdot - \cdot$) superimposed on the slow manifold for different values of ν_p , the maximum plasma membrane $[\text{Ca}^{2+}]_i$ pump rate. Increasing ν_p moves the slow manifold to the right. (A) When $\nu_p = 0.045 \mu\text{M} \cdot \mu\text{m} \cdot \text{ms}^{-1}$ the model exhibits the “fold cycle/fold cycle” bursting in Fig. 2. (B) When $\nu_p = 0.04 \mu\text{M} \cdot \mu\text{m} \cdot \text{ms}^{-1}$ the model reaches a steady state where the $[\text{Ca}^{2+}]_{\text{er}}$ nullcline intersects the slow manifold. (C) When $\nu_p = 0.042 \mu\text{M} \cdot \mu\text{m} \cdot \text{ms}^{-1}$ the model exhibits sustained subthreshold oscillations. (D) When $\nu_p = 0.05 \mu\text{M} \cdot \mu\text{m} \cdot \text{ms}^{-1}$ the model exhibits sustained action potentials and is incapable of bursting.

then attracted towards the smaller stable periodic orbit of Fig. 4 A, and $[\text{Ca}^{2+}]_{\text{er}}$ decreases because $d[\text{Ca}^{2+}]_{\text{er}}/dt < 0$ under the $[\text{Ca}^{2+}]_{\text{er}}$ nullcline ($\cdot - \cdot$). $[\text{Ca}^{2+}]_{\text{er}}$ decreases until a SNP bifurcation occurs when $[\text{Ca}^{2+}]_{\text{er}} = 17.46 \mu\text{M}$, and the small periodic orbit disappears. However the trajectory is not immediately attracted onto the upper stable branch. Small voltage oscillations in the membrane potential of increasing amplitude continue until $[\text{Ca}^{2+}]_{\text{er}}$ decreases to $17.3 \mu\text{M}$, as shown in Fig. 2 A and Fig. 2 C. This slow passage through the SNP bifurcation is similar to the slow passage through a Hopf bifurcation, which is known as the delay or memory effect [Baer et al., 1989, Holden and Erneux, 1993, Arnold et al., 1994]. The process of moving between the two stable periodic branches then repeats, and due to the bifurcations involved, this topological type of bursting is named “fold cycle/fold cycle” bursting [Izhikevich, 2000].

One may ask: What happens if we move the slow manifold relative to the $[\text{Ca}^{2+}]_{\text{er}}$ nullcline? There are two ways to achieve this, we can either move the $[\text{Ca}^{2+}]_{\text{er}}$ nullcline or move the slow manifold. The choice is arbitrary, and we choose to decrease the plasma

membrane $[Ca^{2+}]_i$; maximum pump rate (ν_p) from $0.045 \mu M \cdot \mu m \cdot ms^{-1}$ to $0.04 \mu M \cdot \mu m \cdot ms^{-1}$ to move the slow manifold to the left (see Fig. 4 B). For a spiking system on the upper branch in Fig. 4 B it follows that $[Ca^{2+}]_{er}$ will increase since above the $[Ca^{2+}]_{er}$ nullcline $d[Ca^{2+}]_{er}/dt > 0$. $[Ca^{2+}]_{er}$ will continue to increase until $[Ca^{2+}]_{er} = 15.43 \mu M$, whereupon the action potentials disappear through the upper SNP bifurcation and the system moves onto the smaller stable periodic solution. $[Ca^{2+}]_{er}$ will continue to increase, until the small oscillations die out via a supercritical HB, and a steady state is reached where the $[Ca^{2+}]_{er}$ nullcline intersects the slow manifold at $[Ca^{2+}]_{er} = 16.8 \mu M$.

If the slow manifold is moved slightly to the right by increasing ν_p to $0.042 \mu M \cdot \mu m \cdot ms^{-1}$ then the model behaviour changes (Fig. 4 C). As before $[Ca^{2+}]_{er}$ will increase until the action potentials disappear through a SNP bifurcation, whereupon the system moves onto the smaller stable periodic solution. However the placement of the $[Ca^{2+}]_{er}$ nullcline ensures that the solution remains on the small oscillatory branch with $[Ca^{2+}]_{er}$ increasing to $16.8 \mu M$, which is to the left of the supercritical HB on the lower branch. The model therefore exhibits sustained subthreshold oscillations.

The model behaviour changes again if the slow manifold is moved slightly more to the right by further increasing ν_p to $0.05 \mu M \cdot \mu m \cdot ms^{-1}$ (Fig. 4 D). This time $[Ca^{2+}]_{er}$ increases until $[Ca^{2+}]_{er} = 19.5 \mu M$, which is to the left of the SNP bifurcation on the upper branch. The oscillations therefore remain on the upper branch and the model exhibits sustained action potentials. In Fig. 4 A,C,D the slow manifold lies both above and below the $[Ca^{2+}]_{er}$ nullcline, and hence $[Ca^{2+}]_{er}$ oscillates in phase with the fast subsystem. These oscillations are very small, but are resolvable in Fig. 2 C.

A bifurcation diagram summarising the change in the model dynamics with ν_p is shown in Fig. 5. For $\nu_p = 0.04 \mu M \cdot \mu m \cdot ms^{-1}$ the oscillations decay to a steady state (—) as previously illustrated in Fig. 4 B. As ν_p increases a supercritical HB occurs when $\nu_p = 0.0415 \mu M \cdot \mu m \cdot ms^{-1}$ and the model exhibits small stable oscillations (—). This corresponds to the situation in Fig. 4 C where the placement of the $[Ca^{2+}]_{er}$ nullcline ensures that the solution remains on the small oscillatory branch. A torus bifurcation of limit cycles² (TB) occurs when $\nu_p = 0.0437 \mu M \cdot \mu m \cdot ms^{-1}$, and the model exhibits the “fold cycle/fold cycle” bursting behaviour (---) as illustrated in Fig. 2. This TB corresponds to the moment where left-moving oscillations on the small oscillatory branch in Fig. 4 A meet the lower SNP bifurcation. This mode of bursting continues until $\nu_p = 0.0485 \mu M \cdot \mu m \cdot ms^{-1}$, where another TB occurs and the model exhibits sustained action potentials (—). This corresponds to the situation in Fig. 4 D where the decrease in $[Ca^{2+}]_{er}$ while the action potential is below the $[Ca^{2+}]_{er}$ nullcline precisely balances the increase in $[Ca^{2+}]_{er}$ while the action potential is above the $[Ca^{2+}]_{er}$ nullcline and sustained action potentials occur.

²A torus bifurcation or Neimark-Sacker bifurcation of limit cycles occurs when a closed invariant curve bifurcates from a fixed point of the associated Poincaré map. This closed curve corresponds to a two-dimensional invariant torus.

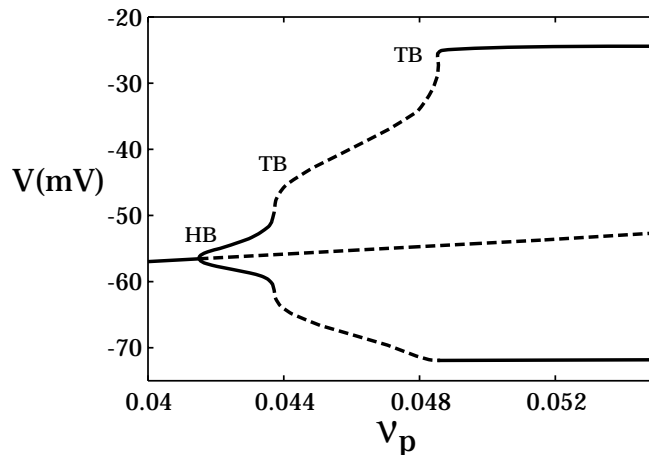


Figure 5: A bifurcation analysis of the model with respect to the maximum plasma membrane $[\text{Ca}^{2+}]_i$ pump rate, ν_p , summarising the sequence of possibilities in Fig. 4. For $\nu_p = 0.04 \mu\text{M} \cdot \mu\text{m} \cdot \text{ms}^{-1}$ the oscillations decay to a stable steady state (—). As ν_p increases a supercritical HB occurs and the model exhibits small stable oscillations (---). A torus bifurcation (TB) occurs when $\nu_p = 0.0437 \mu\text{M} \cdot \mu\text{m} \cdot \text{ms}^{-1}$ and the model exhibits the “fold cycle/fold cycle” bursting behaviour in Fig. 2 (- - -). This “fold cycle/fold cycle” bursting continues until $\nu_p = 0.0485 \mu\text{M} \cdot \mu\text{m} \cdot \text{ms}^{-1}$ where another TB occurs and the model exhibits stable action potentials (—).

5 “Fold cycle/flip” bursting

The bursting in Fig. 2 is similar to a mode of cycle–cycle bursting exhibited in the neuron model of Wang (1993), which was termed “mixed-mode bursting”. In this Hodgkin–Huxley type model the bursting is generated by injecting a current (I_{app}) and modulated by the slow inactivation kinetics of a K^+ current. The slow inactivation gating variable used in that paper is $\rho h_1 + (1 - \rho)h_2$. In order to compare Wang’s model with ours we perform a bifurcation analysis of the model. The model equations and parameters can be found in Wang (1993).

In Fig. 6, a bifurcation analysis with respect to the inactivation variable reveals the model bistability. The quiescent state is a small amplitude subthreshold limit cycle attractor and the spiking state a limit cycle attractor. This diagram shares many of the topological features of the bifurcation diagrams in Fig. 4. Again, the subthreshold limit cycle disappears in a SNP bifurcation but now the spiking limit cycle attractor disappears in a subcritical flip (period doubling) bifurcation (F), and thus is a “fold cycle/flip” burster [Izhikevich, 2000]. This subcritical flip bifurcation results in three unstable periodic solutions (---) for $0.4 \leq \rho h_1 + (1 - \rho)h_2 < 0.402$. Although it is difficult to resolve in Fig. 6, for $0.399 \leq \rho h_1 + (1 - \rho)h_2 < 0.4$ the model exhibits four periodic solutions, one of which is stable (—). Unlike the “fold cycle/fold cycle” burster the “fold cycle/flip” burster cannot occur in models where the fast spiking subsystem is two-dimensional. However, the sharp

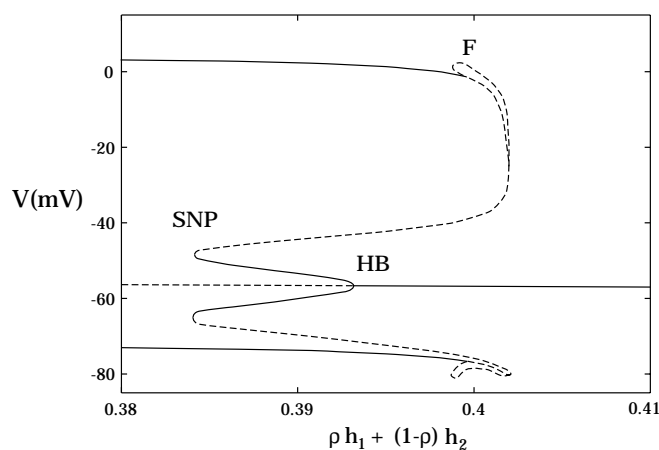


Figure 6: Bifurcation analysis of Wang’s neuron model with respect to the slow inactivation kinetics of a K^+ current. This slow inactivation gating variable is $\rho h_1 + (1 - \rho)h_2$. The bursting is generated by injecting a current ($I_{app} = 3 \mu A \cdot cm^{-2}$). The model is bistable and exhibits “fold cycle/flip” bursting where the subthreshold limit cycle disappears in a SNP bifurcation and the spiking limit cycle attractor disappears in a subcritical flip (period doubling) bifurcation (F). This burster shares many of the topological features of the “fold cycle/fold cycle” burster in Fig. 4 A.

loss in stability of the spiking attractor makes it difficult to distinguish experimentally between the “fold cycle/flip” burster and the “fold cycle/fold cycle” burster.

6 Two parameter bifurcation analysis

The “fold cycle/fold cycle” burster is a variant of the “subHopf/fold cycle” [Izhikevich, 2000] burster, also known as the “elliptic” [Rinzel, 1987] or type III [Bertram et al., 1995] burster. This “subHopf/fold cycle” burster for our model is depicted in Fig. 7, where the quiescent state is a stable equilibrium and the spiking state is a limit cycle attractor. In “subHopf/fold cycle” bursting the rest state disappears in a subcritical Hopf bifurcation and the limit cycle attractor disappears in a fold cycle bifurcation (see Fig. 8 A). Certain changes in our model parameters generate this “subHopf/fold cycle” burster as we now demonstrate by performing a two-parameter bifurcation analysis of the model with respect to the slow variable $[Ca^{2+}]_{er}$, and the leak conductance g_L .

If the leak conductance (g_L) is increased from 0.3 nS to 0.305 nS, then the bifurcation diagram of Fig. 4 B changes to that shown in Fig. 8 A. Note that Fig. 8 is constructed with $\nu_p = 0.04 \mu M \cdot \mu m \cdot ms^{-1}$. This parameter change has taken the model through a codimension-2 Bautin bifurcation ³ (BB) [Kuznetsov, 1998], where the supercritical Hopf

³A Bautin or generalised Hopf bifurcation occurs when the first Lyapunov exponent changes sign while the complex eigenvalues of the linearization remain simple, converting a supercritical Hopf bifurcation into a subcritical one.

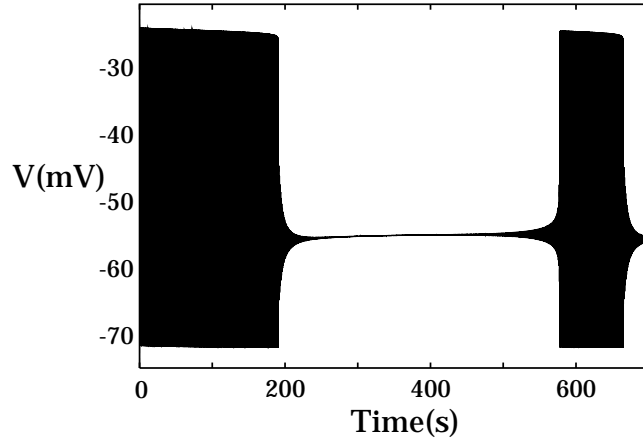


Figure 7: “SubHopf/fold cycle” bursting in the model with $g_L = 0.305$ nS, and $\nu_p = 0.0475 \mu\text{M} \cdot \mu\text{m} \cdot \text{ms}^{-1}$. The active bursting phase begins in a subcritical HB and terminates in the SNP bifurcation of Fig. 8 A.

bifurcation of Fig. 4 B has coalesced with the SNP bifurcation on the lower branch generating the subcritical HB shown in Fig. 8 A. By suitable placement of the $[\text{Ca}^{2+}]_{\text{er}}$ nullcline the model is then capable of exhibiting “subHopf/fold cycle” bursting behaviour by moving between the subcritical HB and the SNP bifurcation. This bursting behaviour is shown in the time domain in Fig. 7. $[\text{Ca}^{2+}]_{\text{er}}$ increases and decreases during the active and silent phases respectively in a similar fashion to that shown in Fig. 2 B, and the $[\text{Ca}^{2+}]_i$ transients mimic the voltage bursting behaviour (not shown).

If g_L is decreased from 0.3 nS to 0.25 nS, then the bifurcation diagram in Fig. 4 B undergoes a different change and is shown in Fig. 8 B. This parameter change has taken the model through a codimension-2 cusp of periodics bifurcation⁴ (CP), where the two SNP bifurcations of Fig. 4 B coalesce and disappear. The model does not now exhibit bistability, and hence is incapable of bursting.

If g_L is further decreased to 0.04 nS, then the bifurcation diagram in Fig. 4 B changes to that in Fig. 8 C. The model has gone through another codimension-2 Bautin bifurcation, where a subcritical HB and a SNP have emerged from the supercritical HB in Fig. 8 B. The model is again capable of exhibiting “subHopf/fold cycle” bursting behaviour by moving between the subcritical HB and the SNP bifurcation (not shown but similar to Fig. 7).

The sequence of bifurcation diagrams in Fig. 8 is summarised by the two-parameter bifurcation diagram in Fig. 9. Curves in the diagram display how the subcritical HB (—), supercritical HB (—), and SNP ($\cdot\cdot\cdot$) bifurcations move with respect to the bifurcation parameters. The three codimension-2 bifurcations separate the two-parameter bifurcation diagram into four regions. Firstly for $g_L > 0.304$ nS, the model is capable of “subHopf/fold cycle” bursting, as shown in Fig. 7. As g_L is decreased a codimension-2 Bautin bifurcation (BB) occurs and for $0.27 < g_L < 0.304$ nS the model is capable of “fold cycle/fold cycle”

⁴A cusp of periodics bifurcation occurs when the three equilibria in the associated Poincaré map, two stable and one unstable, merge together at a cusp point.

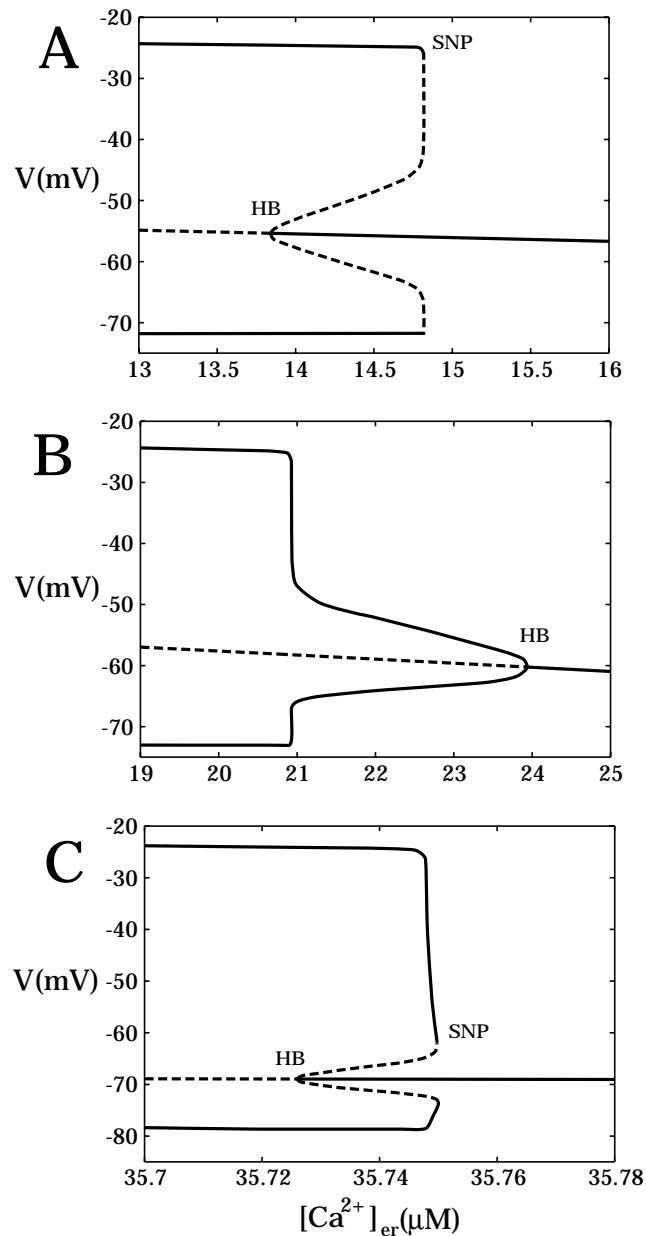


Figure 8: Bifurcation analysis of the model with respect to the slow variable $[\text{Ca}^{2+}]_{\text{er}}$ for different values of the leak conductance g_L . (A) For $g_L = 0.305$ nS a codimension-2 Bautin bifurcation (BB) has occurred where the supercritical HB in Fig. 4 B has coalesced with the SNP on the lower branch generating a subcritical HB. The model can now exhibit “subHopf/fold cycle” bursting, as shown in Fig. 7. (B) For $g_L = 0.25$ nS a codimension-2 cusp of periodics bifurcation (CP) has occurred where the two SNP bifurcations in Fig. 4 B coalesce and disappear. The model is no longer capable of bursting. (C) For $g_L = 0.04$ nS another BB has occurred and the model is again capable of “subHopf/fold cycle” bursting.

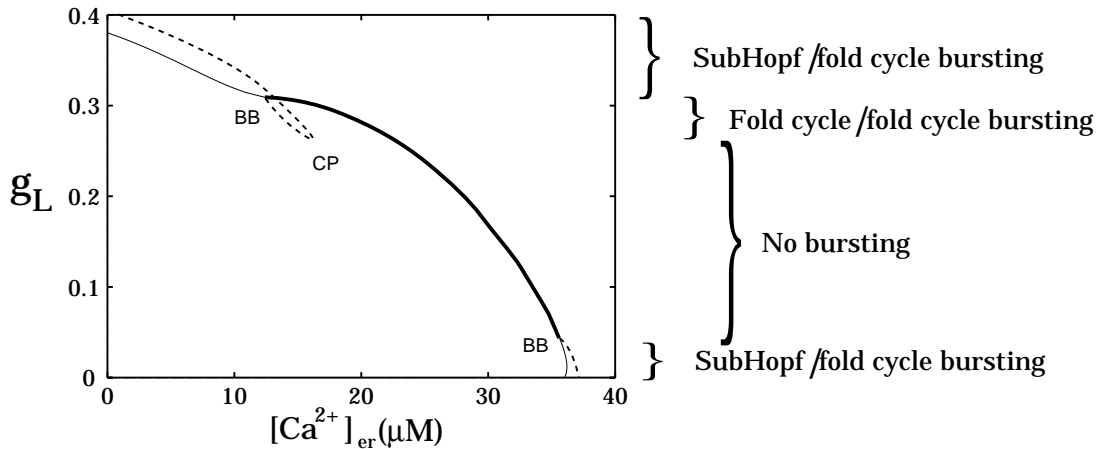


Figure 9: Two-parameter bifurcation analysis of the model with respect to the slow variable $[Ca^{2+}]_{er}$, and the leak conductance g_L . Curves in the diagram display how the supercritical HB (— bold), subcritical HB (— thin), and SNP ($\cdot\cdot\cdot$) bifurcations move with respect to the bifurcation parameters. For $g_L > 0.304$ nS and $g_L < 0.05$ nS the model is capable of “subHopf/fold cycle” bursting. “Fold cycle/fold cycle” bursting occurs for $0.27 < g_L < 0.304$ nS, and for $0.05 < g_L < 0.27$ nS the model is incapable of bursting.

bursting, as shown in Fig. 2. As g_L is further decreased the model undergoes a codimension-2 cusp of periodics bifurcation (CP) when $g_L = 0.27$ nS, and the two SNP bifurcations coalesce and disappear. For $0.05 < g_L < 0.27$ nS the model does not exhibit bistability and hence is incapable of bursting. Another Bautin bifurcation occurs as g_L is further decreased, and for $g_L < 0.05$ nS the model can again generate “subHopf/fold cycle” bursting.

7 Summary

Using a reduced model of corticotroph electrophysiology, we investigated model bursting. The bursting is indirectly driven by slow modulation of the endoplasmic reticulum Ca^{2+} concentration which gives rise to a slow component in $[Ca^{2+}]_i$ and results in electrical bursting via a Ca^{2+} -activated K^+ current. The bursting frequency is dependent on the endoplasmic reticulum Ca^{2+} storage capacity, the Ca^{2+} transport mechanisms, and the activation of a Ca^{2+} -activated K^+ current. This store operated burst modulation mechanism has also been observed in other Hodgkin–Huxley type models [Chay, 1997, Gall and Susa, 1999]. The bursting behaviour can be interpreted as the evolution of a fast oscillatory system through a slow subsystem. Thus, bifurcation theory along with the null-surfaces assist in analysing the bursting mechanism and allow a geometric interpretation of action potential generation.

The model exhibits a novel form of bursting due to bistability between two stable oscillatory solutions. Due to the bifurcations involved, this type of bursting is named “fold cycle/fold cycle” bursting [Izhikevich, 2000], and is topologically equivalent to flow on a

two-dimensional torus. The “fold cycle/fold cycle” bursting behaviour can be interpreted as a variant of the “subHopf/fold cycle” burster, and changes in the underlying model topology allow the model to exhibit this mode of bursting. We have investigated transitions between these different modes of bursting using bifurcation theory.

The model bursting is similar to a mode of cycle–cycle bursting exhibited in the neuron model of Wang (1993). However, in this later model the bursting is modulated by the slow inactivation kinetics of a K^+ current. A bifurcation analysis with respect to this inactivation variable reveals that the spiking state disappears in subcritical flip bifurcation, and thus is a “fold cycle/flip” burster. This mode of bursting shares many of the topological features of the “fold cycle/fold cycle” burster and has also not previously been observed in a Hodgkin–Huxley type model.

This paper aims to highlight interesting modes of bursting in Hodgkin–Huxley type models and the underlying mechanisms. In particular it illustrates how slight parameter changes can lead to quite complex changes in the model behaviour. Many interesting questions regarding the physiological significance of the different bursting modes, and their use in distinguishing bursters experimentally remain to be resolved.

Acknowledgements

We thank Drs A. P. LeBeau, A. B. Robson, and A. E. McKinnon for helpful discussions regarding corticotrophs, and Dr A. J. Sneyd for motivating us to perform this study. We also sincerely thank the journal reviewers for their valuable comments and suggestions. This work was supported by grants from the Marsden Fund administered by the Royal Society of New Zealand, and (PRS) acknowledges the receipt of a University of Canterbury doctoral scholarship.

Appendix: Equations and parameter values

The full seven-variable model equations for the excitable corticotroph cell are as follows:

Ionic currents

$$\begin{aligned}
 c_m \frac{dV}{dt} &= -(I_{Ca-L} + I_{Ca-T} + I_{K-DR} + I_{K-Ca} + I_{Leak}) \\
 I_{Ca-L} &= g_{Ca-L} m_L^2 \phi_{Ca} \\
 I_{Ca-T} &= g_{Ca-T} m_T^2 h_T \phi_{Ca} \\
 I_{K-DR} &= g_{K-DR} n \phi_K \\
 I_{K-Ca} &= g_{K-Ca} \frac{[Ca^{2+}]_i^4}{[Ca^{2+}]_i^4 + K_c^4} \phi_K \\
 I_{Leak} &= g_L (V - V_L) \\
 \phi_j &= V \frac{[j]_i - [j]_e \exp[-z_j FV/(RT)]}{1 - \exp[-z_j FV/(RT)]}, \quad j \in \{Ca^{2+}, K^+\},
 \end{aligned}$$

Gating variables

$$\begin{aligned}\tau_x \frac{dx}{dt} &= x_\infty - x, \quad x \in \{m_L, m_T, h_T, n\} \\ x_\infty &= \frac{1}{1 + \exp[(V_x - V)/k_x]}, \quad x \in \{m_L, m_T, n\} \\ h_{T\infty} &= \frac{1}{1 + \exp[(V - V_{h_T})/k_{h_T}]} \\ \tau_x(V) &= \frac{\bar{\tau}_x}{\exp[(V - V_\tau)/k_\tau] + 2 \exp[2(V_\tau - V)/k_\tau]}, \quad x \in \{m_L, m_T\}\end{aligned}$$

ER Ca^{2+} equations

$$\begin{aligned}\frac{d[\text{Ca}^{2+}]_{\text{er}}}{dt} &= -\frac{f_{\text{er}}}{V_{\text{er}}}(J_{\text{rel}} - J_{\text{up}}) \\ J_{\text{rel}} &= P([\text{Ca}^{2+}]_{\text{er}} - [\text{Ca}^{2+}]_{\text{i}}) \\ J_{\text{up}} &= \frac{\nu_{\text{er}}[\text{Ca}^{2+}]_{\text{i}}^2}{[\text{Ca}^{2+}]_{\text{i}}^2 + K_{\text{er}}^2}\end{aligned}$$

Cytosolic Ca^{2+} equations

$$\begin{aligned}\frac{d[\text{Ca}^{2+}]_{\text{i}}}{dt} &= \frac{f_{\text{cyt}}}{V_{\text{c}}}(J_{\text{rel}} - J_{\text{up}}) + f_{\text{cyt}}\beta(J_{\text{in}} - J_{\text{eff}}) \\ J_{\text{in}} &= -\alpha(I_{\text{Ca-L}} + I_{\text{Ca-T}}) \\ J_{\text{eff}} &= \frac{\nu_{\text{p}}[\text{Ca}^{2+}]_{\text{i}}^2}{[\text{Ca}^{2+}]_{\text{i}}^2 + K_{\text{p}}^2}\end{aligned}$$

The parameter values in the model are listed in Table 2. Source code for our model suitable for running on XPPAUT is available from the authors.

References

- [Adler et al., 1983] Adler, M., B. S. Wong, S. L. Sabol, N. Busis, M. B. Jackson, and F. F. Weight (1983). Action potentials and membrane ion channels in clonal anterior pituitary cells. *Proc. Natl. Acad. Sci. USA* 80:2086–2090.
- [Alberts et al., 1983] Alberts, B., D. Bray, J. Lewis, M. Kaff, K. Roberts, and J. D. Watson (1983). *Molecular Biology of the Cell*. Garland, New York, 1st edition.
- [Arnold et al., 1994] Arnold, V., V. Afrajmovich, Y. Il'yashenko, and L. Shil'nikov (1994). Dynamical Systems V, chapter 4.4. *Encyclopaedia of Mathematical Sciences*. Springer-Verlag, New York.
- [Baer et al., 1989] Baer, S., T. Erneux, and J. Rinzel (1989). The slow passage through a Hopf bifurcation: delay, memory effects, and resonance. *SIAM. J. Appl. Math.* 49:55–71.

Parameter	Definition	Value	Source
c_m	Cell membrane capacitance	7 pF	$1\mu\text{F} \cdot \text{cm}^{-2} \cdot A_{\text{cell}}$
d_{cell}	Cell diameter	15 μm	[LeBeau et al., 1997]
V_{cell}	Cell volume	1.77 pL	$1/6\pi d_{\text{cell}}^3$
V_c	Cytosolic volume	0.85 V_{cell}	[Alberts et al., 1983]
V_{er}	ER volume	0.15 V_{cell}	[Alberts et al., 1983]
A_{cell}	Cell surface area	707 μm^2	πd_{cell}^2
f_{cyt}	Cytosolic Ca^{2+} buffering factor	0.01	[Neher and Augustine, 1992]
f_{er}	ER Ca^{2+} buffering factor	0.0025	[Li et al., 1997]
α	Ca^{2+} current to flux density conversion factor	$0.0074 \mu\text{M} \cdot \mu\text{m} \cdot \text{ms}^{-1} \cdot \text{pA}^{-1}$	$1/(z_{\text{Ca}} F A_{\text{cell}})$
β	Ratio of cell surface area to cytosolic volume	$0.47 \mu\text{m}^{-1}$	A_{cell}/V_c
P	ER permeability	$0.0012 \text{pL} \cdot \text{ms}^{-1}$	[Shorten et al., 1999a]
ν_{er}	Maximum ER Ca^{2+} -ATPase current	$0.05 \mu\text{M} \cdot \text{pL} \cdot \text{ms}^{-1}$	[Shorten et al., 1999a]
K_{er}	$[\text{Ca}^{2+}]_i$ for half maximal pump activity	0.2 μM	[Li et al., 1997]
ν_{p}	Maximum plasma membrane Ca^{2+} -ATPase flux	$0.045 \mu\text{M} \cdot \mu\text{m} \cdot \text{ms}^{-1}$	[LeBeau et al., 1997]
K_{p}	$[\text{Ca}^{2+}]_i$ for half maximal pump activity	0.08 μM	[LeBeau et al., 1997]
V_{mL}	midpoint L-type Ca^{2+} channel activation	-18 mV	[Kuryshv et al., 1995]
$[\text{Ca}^{2+}]_e$	Extracellular $[\text{Ca}^{2+}]$	20 mM	[Guérineau et al., 1991]
$[\text{K}^+]_e$	Extracellular $[\text{K}^+]$	5.6 mM	[Guérineau et al., 1991]
$[\text{K}^+]_i$	Intracellular $[\text{K}^+]$	140 mM	[Li et al., 1995]
g_{L}	Leak conductance	0.3 nS	[LeBeau et al., 1997]
$g_{\text{Ca-L}}$	L-type conductance	$9 \text{nS} \cdot \text{mM}^{-1}$	[Guérineau et al., 1991]
$g_{\text{Ca-T}}$	T-type conductance	$10 \text{nS} \cdot \text{mM}^{-1}$	[Guérineau et al., 1991]
$g_{\text{K-DR}}$	K-DR conductance	$0.1 \text{nS} \cdot \text{mM}^{-1}$	[Mollard et al., 1987]
$g_{\text{K-Ca}}$	K-Ca conductance	$0.09 \text{nS} \cdot \text{mM}^{-1}$	[Mollard et al., 1987]
K_{c}	$[\text{Ca}^{2+}]_i$ for half maximal K-Ca activation	0.4 μM	[LeBeau et al., 1997]
V_{mT}	Midpoint T-type Ca^{2+} channel activation	-30 mV	[Guérineau et al., 1991]
V_{L}	Leak current reversal potential	-67 mV	[LeBeau et al., 1997]
V_{T}	Midpoint of time factor	-60 mV	[Li et al., 1995]
V_{n}	Midpoint K-DR channel activation	-20 mV	[Mollard et al., 1987]
V_{hT}	Midpoint T-type Ca^{2+} channel inactivation	-57 mV	[Guérineau et al., 1991]
k_{mL}	Slope factor for L-type Ca^{2+} channel activation	12 mV	[Kuryshv et al., 1995]
k_{mT}	Slope factor for T-type Ca^{2+} channel activation	10.5 mV	[Guérineau et al., 1991]
k_{hT}	Slope factor for T-type Ca^{2+} channel inactivation	5 mV	[Guérineau et al., 1991]
k_{n}	Slope factor for K-DR activation	4.5 mV	[Mollard et al., 1987]
k_{τ}	Slope factor for time factor	22 mV	[Li et al., 1995]
$\bar{\tau}_{\text{mL}}$	L-type Ca^{2+} channel activation time constant	27 ms	[Kuryshv et al., 1995]
$\bar{\tau}_{\text{mT}}$	T-type Ca^{2+} channel activation time constant	10 ms	[Li et al., 1995]
$\bar{\tau}_{\text{hT}}$	T-type Ca^{2+} channel inactivation time constant	15 ms	[Li et al., 1995]
τ_{n}	K-DR activation time constant	20 ms	[LeBeau et al., 1997]

Table 2: Model parameter values.

[Bertram et al., 1995] Bertram, R., M. J. Butte, T. Kiemel, and A. Sherman (1995). Topological and phenomenological classification of bursting oscillations. *Bulletin of Mathematical Biology* 57:413–439.

[Chay, 1997] Chay, T. (1997). Effects of extracellular calcium on electrical bursting and intracellular and luminal calcium oscillations in insulin secreting pancreatic β -cells. *Biophysical Journal* 73:1673–1688.

[de Vries, 1998] de Vries, G. (1998). Multiple bifurcations in a polynomial model of bursting oscillations. *J. Nonlinear Sci.* 8:281–316.

[Doedel, 1981] Doedel, E. (1981). A program for the automatic bifurcation analysis of autonomous systems. *Congr. Numer.* 30:265–484.

- [Gall and Susa, 1999] Gall, D. and I. Susa (1999). Effect of Na/Ca exchange on plateau fraction and $[Ca]_i$ in models for bursting in pancreatic β -cells. *Biophysical Journal* 77:45–53.
- [Guérineau et al., 1991] Guérineau, N. C., J. B. Corcuff, P. Mariot, B. T. Lussier, and P. Mollard (1991). Spontaneous and corticotropin-releasing factor-induced cytosolic calcium transients in corticotrophs. *Endocrinology*. 129:409–420.
- [Hale and Kocak, 1991] Hale, J. and H. Kocak (1991). Dynamics and Bifurcations, chapter 6. Springer-Verlag.
- [Hodgkin and Huxley, 1952] Hodgkin, A. L. and A. F. Huxley (1952). A quantitative description of membrane current and its application to conduction and excitation in nerve. *J. Physiol. (Lond)*. 117:500–544.
- [Holden and Erneux, 1993] Holden, L. and T. Erneux (1993). Slow passage through a Hopf bifurcation: from oscillatory to steady state solutions. *SIAM J. Appl. Math.* 53:1045–1058.
- [Izhikevich, 2000] Izhikevich, E. (2000). Neural excitability, spiking and bursting. *International Journal of Bifurcation and Chaos* 10:In Press.
- [Kuryshv et al., 1995] Kuryshv, Y. A., G. V. Childs, and A. K. Ritchie (1995). Three high threshold calcium channel subtypes in rat corticotrophs. *Endocrinology*. 136:3916–3924.
- [Kuryshv et al., 1996] Kuryshv, Y. A., G. V. Childs, and A. K. Ritchie (1996). Corticotropin-releasing hormone stimulates Ca^{2+} entry through L- and P-type Ca^{2+} channels in rat corticotrophs. *Endocrinology*. 137:2269–2277.
- [Kuryshv et al., 1997] Kuryshv, Y. A., L. Haak, G. V. Childs, and A. K. Ritchie (1997). Corticotropin releasing hormone inhibits an inwardly rectifying potassium current in rat corticotrophs. *J. Physiol. (Lond)*. 502.2:265–279.
- [Kuznetsov, 1998] Kuznetsov, Y. A. (1998). Elements of Applied Bifurcation Theory. Springer-Verlag, 2nd edition.
- [LeBeau et al., 1997] LeBeau, A. P., A. B. Robson, A. E. McKinnon, R. A. Donald, and J. Sneyd (1997). Generation of action potentials in a mathematical model of corticotrophs. *Biophys. J.* 73:1263–1275.
- [LeBeau et al., 1998] LeBeau, A. P., A. B. Robson, A. E. McKinnon, and J. Sneyd (1998). Analysis of a reduced model of corticotroph action potentials. *J. theor. Biol.* 192:319–339.
- [Li et al., 1995] Li, Y., J. Rinzel, L. Vergara, and S. Stojilković (1995). Spontaneous electrical and calcium oscillations in unstimulated pituitary gonadotrophs. *Biophys. J.* 69:785–795.
- [Li et al., 1997] Li, Y., S. Stojilković, J. Keizer, and J. Rinzel (1997). Sensing and refilling calcium stores in an excitable cell. *Biophys. J.* 72:1080–1091.
- [Mollard et al., 1987] Mollard, P., N. C. Guérineau, J. Audin, and B. Dufy (1987). Electrical properties of cultured human adrenocorticotropin-secreting adenoma cells: effects of high K^+ , corticotropin-releasing factor, and angiotensin II. *Endocrinology*. 121:395–405.

- [Neher and Augustine, 1992] Neher, E. and G. J. Augustine (1992). Calcium gradients and buffers in bovine chromaffin cells. *J. Physiol. (Lond)*. 450:273–301.
- [Rinzel, 1985] Rinzel, J. (1985). Bursting oscillations in an excitable membrane model. In B. Sleeman and R. Jarvis, editors, *Proc. 8th Dundee Conference on the Theory of Ordinary and Partial Differential Equations*. Springer-Verlag, New York.
- [Rinzel, 1987] Rinzel, J. (1987). A formal classification of bursting mechanisms in excitable systems. In E. Teramoto and M. Yamaguti, editors, *Mathematical Topics in Population Biology, Morphogenesis and Neurosciences*, volume 71 of *Lecture Notes in Biomathematics*. Springer-Verlag, Berlin.
- [Rinzel and Lee, 1986] Rinzel, J. and Y. Lee (1986). On different mechanisms for membrane potential bursters. In H. Othmer, editor, *Nonlinear Oscillations in Biology and Chemistry*, volume 66 of *Lecture Notes in Biomathematics*. Springer-Verlag, New York.
- [Rush and Rinzel, 1994] Rush, M. and J. Rinzel (1994). Analysis of bursting in a thalamic neuron model. *Biological Cybernetics* 71:281–291.
- [Shorten et al., 1999a] Shorten, P. R., A. P. LeBeau, A. B. Robson, A. E. McKinnon, and D. J. N. Wall (1999a). A role of the endoplasmic reticulum in a mathematical model of corticotroph action potentials. Technical Report 173/1-21/(1999), University of Canterbury, New Zealand.
- [Shorten et al., 1999b] Shorten, P. R., A. B. Robson, A. E. McKinnon, and D. J. N. Wall (1999b). The inward rectifier in a model of corticotroph electrical activity. Technical Report 185/1-22/(1999), University of Canterbury, New Zealand.
- [Wang, 1993] Wang, X. (1993). Ionic basis for intrinsic 40 Hz neuronal oscillations. *NeuroReport* 5:221–224.